



## An improved multiaxial rainflow algorithm for non-proportional stress or strain histories – Part II: The Modified Wang–Brown method

Marco Antonio Meggiolaro\*, Jaime Tupiassú Pinho de Castro

Department of Mechanical Engineering, Pontifical Catholic University of Rio de Janeiro, Rua Marquês de São Vicente 225 – Gávea, Rio de Janeiro, RJ 22453-900, Brazil

### ARTICLE INFO

#### Article history:

Received 1 November 2010  
Received in revised form 2 August 2011  
Accepted 28 October 2011  
Available online 17 November 2011

#### Keywords:

Multiaxial fatigue  
Non-proportional loadings  
Enclosing surface methods  
Wang–Brown algorithm  
Multiaxial rainflow algorithms

### ABSTRACT

The objective of this work is to develop a simple multiaxial rainflow algorithm that allows the proper calculation of multiaxial damage in NP histories. Enclosing surface methods are usually employed to obtain the equivalent ranges necessary for damage calculation, as discussed in Part I of this 2-part paper. Part I also presented a new approach to evaluate equivalent ranges in NP histories, called the Moment Of Inertia (MOI) method. This second and last part presents a multiaxial rainflow counting algorithm that allows the MOI and enclosing surface methods to be generalized to non-periodic NP histories and to periodic NP histories formed by complex blocks with multiple cycles each. It is shown that Wang–Brown's (WB) multiaxial rainflow algorithm has a few idiosyncrasies that can lead to non-conservative predictions, incorrectly filtering out significant events within a multiaxial loading cycle. An improved multiaxial rainflow algorithm is proposed, called Modified Wang–Brown (MWB). It has two main improvements over the WB algorithm. First, the criterion to choose the point where the count is started is modified. Examples are shown to prove that the original criterion can overlook the most damaging event from the history, as opposed to the modified version. And second, the algorithm implementation is significantly simplified when formulated in a reduced five-dimensional Euclidean space. Under plane stress conditions, the algorithm is further simplified using a three-dimensional Euclidean space based on the deviatoric stresses or strains. A simple pseudo-code is presented in a flowchart to efficiently implement the multiaxial count, allowing a fast and efficient calculation of fatigue damage even for very long non-periodic NP histories.

© 2011 Elsevier Ltd. All rights reserved.

### 1. Introduction

Non-proportional (NP) multiaxial fatigue life predictions require the use of a multiaxial rainflow algorithm together with a method to calculate the effective stress or strain ranges associated with each counted cycle [1]. Part I of this paper presented several methods to compute the equivalent stress or strain ranges in non-proportional (NP) multiaxial histories. It compared all existing enclosing surface methods based on more than  $3 \times 10^6$  Monte Carlo simulations of different path topologies in two to five-dimensional stress or strain diagrams. New enclosing surface models were also proposed, based on Deperrois' idea of longest chords [2].

A new method to calculate equivalent ranges in NP histories was also presented in Part I, called the Moment Of Inertia (MOI) method. The MOI method is not based on enclosing surfaces. It is useful to obtain the equivalent stress or strain ranges and mean component of the NP path. Experimental results for 13 different multiaxial histories from [3] proved the effectiveness of the MOI method to pre-

dict the associated fatigue lives. The MOI method can be used even in complex-shaped paths such as the ones studied in [4], as long as it is coupled with a multiaxial rainflow count such as the one from Wang–Brown [5] applied to a sub-space of a reduced five-dimensional Euclidean space [6]. The experiments presented in Part I were also used to evaluate the enclosing surface methods.

The equivalent ranges predicted by the MOI or enclosing surface methods are needed by most multiaxial fatigue damage models, such as the ones proposed by Sines [7], Crossland [8], Findley [9], McDiarmid [10,11], Brown–Miller [12], Fatemi–Socie [13], and by the Smith–Watson–Topper (SWT) model [14]. A generic NP history should be projected onto a candidate plane, and then counted using a multiaxial rainflow algorithm to identify individual cycles [15]. For each counted cycle or half-cycle, the equivalent range can be computed using enclosing surface methods [16–20], which try to find circles, ellipses or rectangles that contain the entire path (in the 2D case). Another promising method to compute equivalent ranges was presented in Part I of this paper, the so-called Moment Of Inertia (MOI) method, which calculates the ranges and mean components of a given history path in a 2D deviatoric stress or strain space.

However, in the form presented in Part I, these methods are only applicable to periodic histories or to infinite life calculations.

\* Corresponding author. Tel.: +55 21 3527 1424; fax: +55 21 3527 1165.

E-mail addresses: [meggi@puc-rio.br](mailto:meggi@puc-rio.br) (M.A. Meggiolaro), [jtcastro@puc-rio.br](mailto:jtcastro@puc-rio.br) (J.T.P. de Castro).

Finite life calculations can be performed, but usually the available models implicitly assume that each block of the periodic loading path contains a single cycle. To generalize the existing methods to finite life predictions in periodic histories with multiple cycles at each block or period, or to non-periodic histories, a cycle counting algorithm must be introduced.

The rainflow algorithm [21,22] is reputedly the best approach to identify the most damaging events embedded in a variable amplitude (VA) history. For linear elastic uniaxial histories, it is indifferent to perform the uniaxial rainflow count on the stresses or on the strains. In addition, the sequential (ordered) rainflow count is always a better option over the traditional rainflow, since it preserves the original loading order. The sequential rainflow is obtained by simply reordering the resulting traditional rainflow count by the final counting point [23,24]. Even for linear elastic problems, where the damage caused by each event should not depend on the other events nor on the loading order, it is a good idea to choose the sequential rainflow to correctly predict in which event the accumulated damage reaches its critical value (usually 1.0, according to Miner [25]). The use of a sequential rainflow count is also recommended for crack growth predictions, to correctly account for load interaction effects without changing the load order.

For elastoplastic uniaxial histories, it is fundamental to calculate the hysteresis loops before performing any rainflow count. After measuring/calculating both stress and strain histories, the sequential rainflow count must be applied to the strains, never to the stresses. The reason for that can be seen in Fig. 1.

The sequential rainflow count of the stresses from the original loading  $\{A \rightarrow B \rightarrow C \rightarrow D\}$  from Fig. 1(i) would result in the half-cycles  $AB, BC$  and  $CD$ . The strain range  $\Delta\varepsilon_{AD}$  from the  $AD$  half-cycle is certainly the most damaging in that history, however this half-cycle was not identified in such stress count. Since the strain range is the most relevant quantity in damage calculation under elastoplastic strains, the sequential rainflow must be performed on the strains (not stresses), resulting in the correct half-cycles  $CB, BC$  and  $AD$ . Fig. 1(ii) provides another example, where the rainflow of stresses would wrongfully predict the half-cycles  $AB, BC$  and  $CD$ , while the rainflow of strains would lead to the expected  $CB, BC$  and  $AD$ .

However, even for uniaxial loads, the rainflow of strains does not always pick up the most damaging events. Two notable excep-

tions are shown in Fig. 1(iii) and (iv). In Fig. 1(iii), both rainflow of strains and stresses would result in the half-cycles  $AB, BC$  and  $CD$ , where  $CD$  should be the most damaging event due to its higher strain range  $\Delta\varepsilon_{CD}$ . This count is correct if the Smith–Watson–Topper (SWT) damage model is used [14], because its damage parameter  $\sigma_{max} \cdot \Delta\varepsilon/2 = \sigma_D \cdot \Delta\varepsilon_{CD}/2$  is indeed maximum at the half-cycle  $CD$ , since both stress  $\sigma_D$  at point  $D$  and strain range  $\Delta\varepsilon_{CD}$  are the highest in the history.

But, if the Morrow damage models are used [1], the maximum damage would probably be associated with the half-cycle  $AD$ . Although the strain range  $\Delta\varepsilon_{AD}$  is slightly smaller than  $\Delta\varepsilon_{CD}$  in Fig. 1(iii), the mean stress  $\sigma_{m,AD} = \sigma_D/2$  in  $AD$  is much higher than the mean stress  $\sigma_{m,CD} = (\sigma_C + \sigma_D)/2$  in  $CD$ . If the compressive deformation at point  $C$  is close to zero, then according to Morrow the combination of  $\Delta\varepsilon_{AD}$  and  $\sigma_{m,AD}$  will result in a higher damage than the combination  $\Delta\varepsilon_{CD}$  and  $\sigma_{m,CD}$ . So, a rainflow count of the damage parameters, which would try to find the events associated with the highest damages and consequently the maximum accumulated damage, would result in the half-cycles  $CB, BC$  and  $AD$  for the Morrow damage models. But, for the SWT damage model, the rainflow of damage parameters would agree with the rainflow of strains, resulting in  $AB, BC$  and  $CD$ . In summary, the rainflow count may depend on the adopted damage model, a problem not as well reported as it should.

The other notable exception where the rainflow of strains may not pick up the most damaging event from a uniaxial history is shown in Fig. 1(iv). In this case, the rainflow of strains results in the half-cycles  $CB, BC$  and  $AD$ , while the rainflow of stresses obtains  $AB, BC$  and  $CD$ . If the compressive deformation at point  $C$  is close to zero, then the strain range  $\Delta\varepsilon_{CD}$  will be very close to  $\Delta\varepsilon_{AD}$ . But both mean stress  $\sigma_{m,CD}$  and maximum stress  $\sigma_C$  from  $CD$  are much higher than, respectively, the mean stress  $\sigma_{m,AD}$  and maximum stress  $\sigma_A = 0$  from  $AD$ , as seen in Fig. 1(iv). Therefore, the Morrow and even the SWT damage models would predict  $CD$  as the most damaging event. This would imply that the maximum accumulated damage would be associated with the count  $AB, BC$  and  $CD$ , which would not agree with the rainflow of strains.

Fortunately, for uniaxial histories, in practice the possibly inaccurate fatigue life calculated from the rainflow of strains is very close to the (correct) life from the rainflow of damage parameters. The two notable exceptions discussed above must involve the initial point  $A$  from the entire loading history, therefore this miscalculated damage problem can only affect a single half-cycle from the

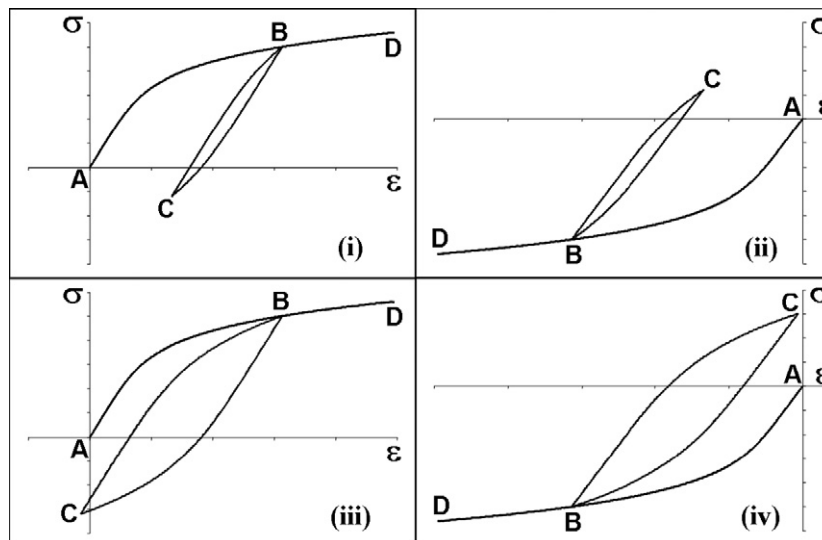


Fig. 1. Examples of uniaxial hysteresis loops.

entire load history (the half-cycle that includes point A). So, even though the (miscalculated) damage from using the rainflow of strains may be much lower than the actual damage value, its influence on the total initiation life should be small. Nevertheless, these issues are an indication that rainflow algorithms can lead to inaccurate predictions if not fully understood.

In summary, for the uniaxial linear elastic case, the traditional or sequential rainflow of stresses, strains or damage parameters result in the same count, therefore any of them can be used in the SN method without problems. But the rainflow of stresses is not appropriate in the presence of plastic strains. In this case, the sequential rainflow of strains should be used in the uniaxial elasto-plastic case.

For multiaxial problems, however, the uniaxial rainflow of stresses or strains may lead to significant errors, even in the linear elastic case, as discussed in the next section.

**2. Rainflow of a simple proportional biaxial load history**

The limitations of the uniaxial rainflow algorithm when dealing with multiaxial loadings can be seen in the following example: calculate the rainflow count that maximizes the accumulated damage, according to the SWT model [14], of a biaxial history consisting of 100 consecutive loading blocks of the 2 cycles  $(\sigma_x, \sigma_y) = \{(0,0), (300,-300), (-100,-360), (400,120), (0,0)\}$  MPa, using Young modulus  $E = 200$  GPa, yield strength  $S_Y = 500$  MPa, and Poisson coefficient  $\nu_{el} = 1/3$ .

Since the stresses in this simple proportional load history are always below  $S_Y$ , the strains  $\epsilon_x$  and  $\epsilon_y$  will be assumed elastic, obtained from Hooke's law

$$\begin{aligned} \epsilon_x &= (\sigma_x - \nu \cdot \sigma_y) / E = \{0, 2, 0.1, 1.8, 0\} \cdot 10^{-3} \\ \epsilon_y &= (\sigma_y - \nu \cdot \sigma_x) / E \cong \{0, -2, -1.63, -0.067, 0\} \cdot 10^{-3} \end{aligned} \tag{1}$$

There is no need to rainflow count the entire strain history. It is enough to perform the rainflow count on a window of two consecutive cycles of the entire history, replicating the result for the remaining identical blocks. Note, however, that such window must begin on the lowest valley  $\epsilon_{low}$  or on the highest peak  $\epsilon_{high}$  of the loading block to be able to fully identify the largest cycle  $\epsilon_{low} \rightarrow \epsilon_{high} \rightarrow \epsilon_{low}$ .

For the damage calculation problem in the  $x$  direction, the original block coincidentally starts at the lowest valley  $\epsilon_{x,low} = 0$ , so the (sequential) rainflow count of the strains  $\epsilon_x$  can begin at point A in Fig. 2, resulting in the paths AB, DC, CD and BCC'E. Both paths AB and BCC'E result in  $\Delta\epsilon_x = 2.0 \times 10^{-3}$ ,  $\sigma_{x,max} = \sigma_{x,B} = 300$  MPa, and a SWT damage parameter  $\sigma_{x,max} \cdot \Delta\epsilon_x / 2 = 0.3$ , while both paths DC and CD give  $\Delta\epsilon_x = 1.7 \times 10^{-3}$ ,  $\sigma_{x,max} = \sigma_{x,D} = 400$  MPa, and a SWT damage parameter  $\sigma_{x,max} \cdot \Delta\epsilon_x / 2 = 0.34$ .

Now, assume that each block of this linear elastic load history was applied backwards, i.e., in the order  $E \rightarrow D \rightarrow C \rightarrow B \rightarrow A$ . In theory, there is no reason for the accumulated damage to be different than the one from the original (forward) history, unless closure effects are introduced in the crack initiation modeling. But, in this reverse order from E to A, the (sequential) rainflow count of the  $\epsilon_x$  strains results in paths EDD'B, DC, CD' and BA, where D' is also defined in Fig. 2. Path EDD'B results in  $\Delta\epsilon_x = 2.0 \times 10^{-3}$ ,  $\sigma_{x,max} = \sigma_{x,D} = 400$  MPa, and a SWT damage parameter  $\sigma_{x,max} \cdot \Delta\epsilon_x / 2 = 0.4$ ; path DC gives  $\Delta\epsilon_x = 1.7 \times 10^{-3}$ ,  $\sigma_{x,max} = \sigma_{x,D} = 400$  MPa, and a SWT damage parameter  $\sigma_{x,max} \cdot \Delta\epsilon_x / 2 = 0.34$ ; path CD' gives  $\Delta\epsilon_x = 1.7 \times 10^{-3}$ ,  $\sigma_{x,max} = \sigma_{x,D'} = 258$  MPa (obtained from interpolating the graph), and a SWT damage parameter  $\sigma_{x,max} \cdot \Delta\epsilon_x / 2 \cong 0.22$ ; and finally path BA gives  $\Delta\epsilon_x = 2.0 \times 10^{-3}$ ,  $\sigma_{x,max} = \sigma_{x,B} = 300$  MPa, and a SWT damage parameter  $\sigma_{x,max} \cdot \Delta\epsilon_x / 2 = 0.3$ . Note that the maximum stress along a counted path may happen at any location inside it, e.g. at point D for path EDD'B.

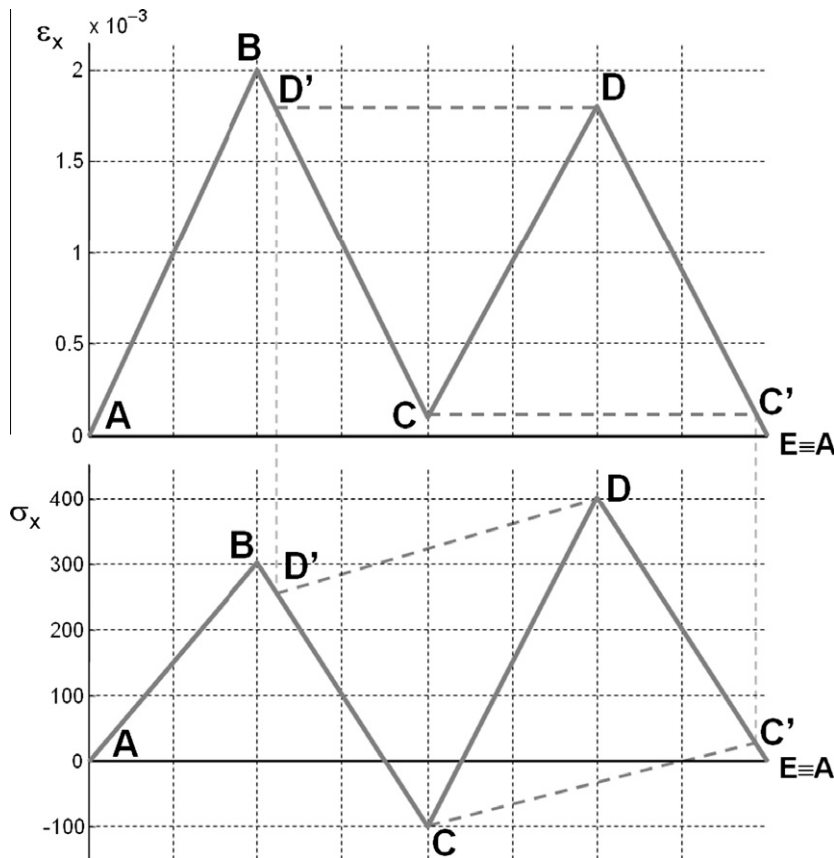


Fig. 2. Strains and stresses in the x direction for each loading block of the biaxial example.

Due to the high non-linear influence of the damage parameter on the SWT model life prediction, it is very likely that the accumulated damage associated with this rainflow count in the reverse order becomes significantly higher than the one from the rainflow in the forward order, mainly due to the contribution of the path  $EDD'B$  and its highest SWT damage parameter 0.4.

So, if  $BCC'E$  is an acceptable (forward) path for the event that starts in  $B$  and ends in  $E$ , with a SWT damage parameter 0.3, then why not consider the alternative forward path  $BD'DE$  (identical to the  $EDD'B$  path, but in the forward direction) associated with the much higher damage parameter 0.4? From this reasoning, the rainflow count in the  $x$  direction that maximizes the SWT damage for the 100 blocks should result in the triplets  $(\Delta\epsilon_x, \sigma_{max}, n) = (2.0 \times 10^{-3}, 400, 50)$ ,  $(1.7 \times 10^{-3}, 400, 50)$ ,  $(1.7 \times 10^{-3}, 258, 50)$ , and  $(2.0 \times 10^{-3}, 300, 50)$ , where  $n$  is the number of cycles.

In summary, the forward rainflow count of the strains does not pick up the most damaging event in this multiaxial example. It is recommended to perform both forward and reverse rainflow counts to choose the one associated with the highest accumulated damage. Even so, there is no guarantee that there would not be another path combination leading to a higher accumulated damage than the one from the forward and reverse counts. This is a significant limitation of the use of a uniaxial rainflow count, even in a simple biaxial history.

Note that the rainflow of stresses  $\sigma_x$  from each loading block, in either forward or reverse direction, would never pick up the event with highest SWT damage parameter 0.4. Note also that the rainflow of  $\sigma_x$  would require the count to start at  $C$  or  $D$  (the lowest valley or highest peak in  $\sigma_x$ ).

But the previous calculations only consider cracks that might initiate in a plane perpendicular to the  $x$  direction. To predict, according to SWT, whether cracks would initiate perpendicular to the  $y$  direction, it is necessary to repeat the calculations for the strains  $\epsilon_y$  and stresses  $\sigma_y$ .

For the damage calculation problem in the  $y$  direction, the rainflow count of the strains must begin at the highest peak  $\epsilon_{y,high} = 0$  at point  $A$  (or at the lowest valley  $\epsilon_{y,low} = -2.0 \times 10^{-3}$  at point  $B$ ), see Fig. 3.

The (sequential) rainflow count of  $\epsilon_y$ , beginning at point  $A$ , results only in the paths  $AB$  and  $BCDE$ . The path  $AB$  results in  $\Delta\epsilon_y = 2.0 \times 10^{-3}$ ,  $\sigma_{y,max} = \sigma_{y,A} = 0$ , and a SWT damage parameter  $\sigma_{y,max} \cdot \Delta\epsilon_y / 2 = 0$ , while path  $BCDE$  gives  $\Delta\epsilon_y = 2.0 \times 10^{-3}$ ,  $\sigma_{y,max} = \sigma_{y,D} = 120$  MPa, and a SWT damage parameter  $\sigma_{y,max} \cdot \Delta\epsilon_y / 2 = 0.12$ . A rainflow count of  $\epsilon_y$  in the reverse path would arrive at the same result. Such low damage parameters in  $y$  indicate that the dominant crack should initiate perpendicular to the  $x$  direction.

Note that the rainflow of stresses  $\sigma_y$  from each loading block would require the count to start at  $C$  or  $D$  (the lowest valley or highest peak in  $\sigma_y$ ), resulting in a quite different count, namely the half-cycles  $CD$  and  $DEABC$ , with a lower SWT damage parameter of 0.094 each.

From this simple example, it can be concluded that, for biaxial histories: (i) the rainflow of strains is much more likely to pick up the most damaging cycle than the rainflow of stresses; (ii) the forward and backward rainflow counts can lead to different accumulated damages, so it is a good idea to perform both; (iii) the rainflow count can give very different loading paths and numbers of counted cycles depending on the direction (e.g. 2 strain cycles

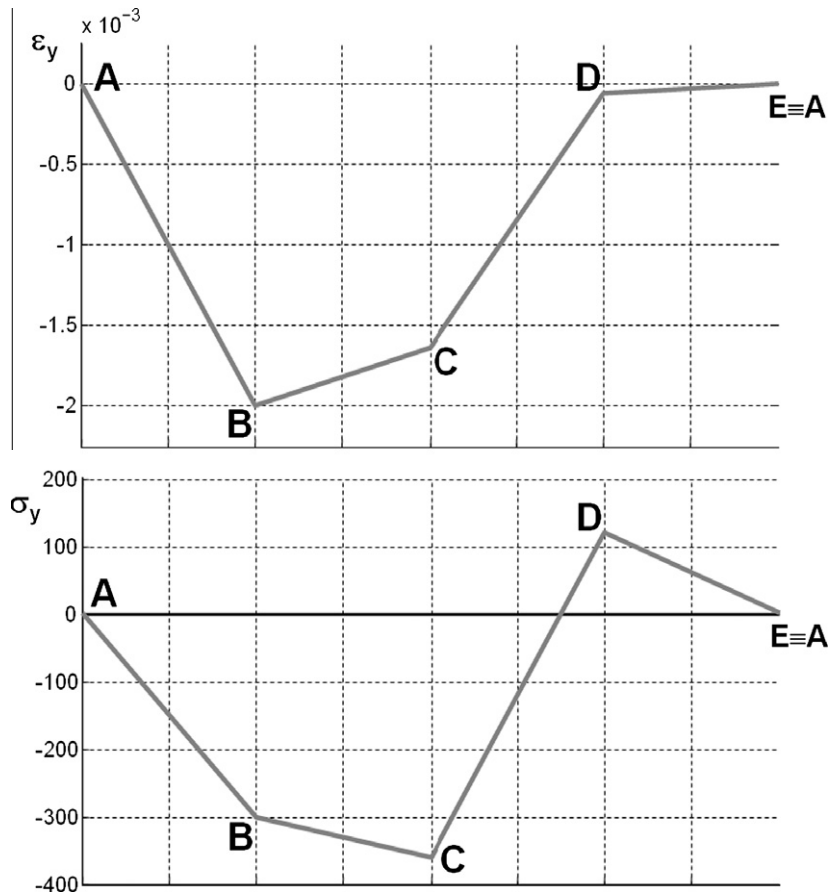


Fig. 3. Strains and stresses in the  $y$  direction for each loading block of the biaxial example.

were counted in the  $x$  direction for every block, while only 1 strain cycle was identified in  $y$ ) and on the chosen quantity to be counted (i.e., rainflow of strains or stresses).

In the next section, the issues involved in applying a rainflow count to a general multiaxial history are discussed.

### 3. Rainflow of a multiaxial history

The uniaxial rainflow approach presented in the previous section was only possible since crack initiation in the  $x$  or  $y$  directions are usually decoupled in a simple biaxial (and therefore proportional) load history. For general NP multiaxial histories, the traditional uniaxial rainflow count, applied to some stress or strain component that is assumed dominant to describe the history, does not provide good life predictions. This is so because the peaks and valleys of the stresses and the corresponding strains do not usually coincide, even in the same direction, not to mention in different directions.

Another important issue involves the common practice of filtering non-reversals from a measured history. When dealing with measured multiaxial loading histories, the sampling points that do not constitute a reversal in any of its stress or strain components are usually eliminated. Filtering points that do not constitute a reversal helps to decrease computational cost in multiaxial fatigue calculations, especially when dealing with over-sampled data [26].

But filtering out all points that do not constitute a reversal in one stress or strain component may cause significant damage prediction problems, discussed next. First, the reversal points obtained from a multiaxial rainflow algorithm may not occur at the reversal of one of the stress or strain components. E.g., the relative Mises strain, used in Wang–Brown's rainflow count, may reach a peak value at a point that is not a maximum or minimum of any strain component. But this most important point would have been filtered out by any non-reversal filtering algorithm, compromising the results.

The second problem may occur because the entire path between two reversals is needed to evaluate the equivalent stress or strain associated with each count, e.g. using an enclosing surface method or the Moment Of Inertia (MOI) method presented in Part I of this paper. Filtering out points along such path would almost certainly result in lower equivalent stress or strain range estimates than expected.

Another issue with rainflow counting NP multiaxial histories is whether or not to use a critical plane approach. The Wang–Brown multiaxial rainflow algorithm is general enough to be directly applied to a multiaxial history involving all six strain components. But the counted cycles will probably occur in different planes, not reproducing the crack initiation mechanism. For instance, if the Wang–Brown rainflow was applied to the biaxial example discussed above, the resulting half-cycles would be obtained based on relative Mises strain quantities that mix the strains in both  $x$  and  $y$  direction, without decoupling their effect, as it would be expected in this case.

Instead, a critical plane approach must be followed: the multiaxial history must be projected onto a candidate plane, and only then should a multiaxial rainflow count be used.

In this critical plane approach, the stress and/or strain history is projected onto a candidate plane from the critical point. A uniaxial rainflow count is then applied to an appropriate strain or stress component, which depends on the chosen damage model: for the  $\varepsilon N$  and SWT [14] damage models, the normal strain perpendicular to the candidate plane is rainflow counted; in the Brown–Miller [12], Fatemi–Socie [13] and Wang–Brown [5] damage models, a shear strain component acting parallel to the candidate plane is

rainflow counted; and in the Findley [9] damage model, a shear stress component parallel to the candidate plane is counted.

While performing such rainflow count on the candidate plane, the other stress and strain components cannot be overlooked or discarded. For instance, if the SWT damage model is used, at every rainflow counted half-cycle  $\varepsilon_1$ , the maximum value of the normal stress  $\sigma_{\perp 1}$  parallel to  $\varepsilon_1$  along the entire half-cycle must be stored to compute  $\sigma_{\perp 1 \max}$  [15]. Since for complex NP multiaxial load histories these maxima may happen at any point along the half-cycle, not only at the peaks and valleys of a given component, non-reversals should never be filtered out before performing the rainflow count.

Note also that, if only the strain (or stress) history is provided, one might need to calculate the entire stress–strain history from proportional multiaxial stress–strain relations or from incremental plasticity techniques, before performing the rainflow count. After performing the rainflow count at each candidate plane, the resulting damage is calculated. The critical plane is then the candidate plane that results in the highest fatigue damage.

However, it must be noted that Case B cracks (defined in Part I of this paper and also in [1]) can have two shear strain (or stress) components acting parallel to each candidate plane. A uniaxial rainflow approach would either neglect the effect of one of such shear components, or consider that one of them is dominant over the other during the rainflow algorithm application [15]. But this practice can be non-conservative, since both shear components induce crack initiation. To deal with that, a true multiaxial rainflow algorithm must be used, accounting for all stress or strain components, such as Wang–Brown's algorithm, discussed next.

### 4. Wang–Brown's multiaxial rainflow algorithm

Wang and Brown [5] proposed an interesting multiaxial generalization of the rainflow count that is applicable to any proportional or NP history of strains (or stresses, with simple modifications to the algorithm). Wang–Brown's multiaxial rainflow is based on the Mises strain  $\varepsilon_{Mises}$  as an indirect measure of fatigue damage.

The problem with using  $\varepsilon_{Mises}$  is the loss of the loading event sign, since Mises values are always positive. Therefore, in 90° out-of-phase histories it is even possible that  $\varepsilon_{Mises}$  remains constant, which would wrongfully result in an infinite life prediction. To solve this issue, the relative Mises strain  $\varepsilon_{RMises}$  is used, calculated from the difference between the strain components  $(\varepsilon_{xj}, \varepsilon_{yj}, \varepsilon_{zj}, \gamma_{xyj}, \gamma_{xzj}, \gamma_{yzj})$  of each ( $j$ )th point in the history and the strain components  $(\varepsilon_{xi}, \varepsilon_{yi}, \varepsilon_{zi}, \gamma_{xyi}, \gamma_{xzi}, \gamma_{yzi})$  of the initial ( $i$ )th point of the current count:

$$\varepsilon_{RMises} = \frac{\sqrt{(\Delta\varepsilon_x - \Delta\varepsilon_y)^2 + (\Delta\varepsilon_x - \Delta\varepsilon_z)^2 + (\Delta\varepsilon_y - \Delta\varepsilon_z)^2 + 1.5(\Delta\gamma_{xy}^2 + \Delta\gamma_{xz}^2 + \Delta\gamma_{yz}^2)}}{\sqrt{2} \cdot (1 + \bar{\nu})} \quad (2)$$

where  $\Delta\varepsilon_x \equiv \varepsilon_{xj} - \varepsilon_{xi}$ ,  $\Delta\varepsilon_y \equiv \varepsilon_{yj} - \varepsilon_{yi}$ ,  $\Delta\varepsilon_z \equiv \varepsilon_{zj} - \varepsilon_{zi}$ ,  $\Delta\gamma_{xy} \equiv \gamma_{xyj} - \gamma_{xyi}$ ,  $\Delta\gamma_{xz} \equiv \gamma_{xzj} - \gamma_{xzi}$ ,  $\Delta\gamma_{yz} \equiv \gamma_{yzj} - \gamma_{yzi}$ , and  $j > i$ .

The relative strains need to be re-calculated for every initial counting point, a computationally intensive task for very long histories. Note however that the relative strain  $\varepsilon_{RMises}$  is only used to locate the initial and final counting points of each half-cycle, after which it is possible to apply at these points any multiaxial damage model (even models that do not include a Mises strain parameter).

As in the uniaxial case, Wang–Brown's multiaxial rainflow is based on three simple rules:

1. The first count must start at the point with the largest value of  $\varepsilon_{Mises}$  from the entire history.

2. Each count must be initiated sequentially at each peak or valley of a strain component, and the relative Mises strain  $\epsilon_{RMises}$  of the subsequent history must be computed with respect to the initial point.
3. The final point of each count is obtained when reaching:
  - (a) the largest value of  $\epsilon_{RMises}$  with respect to the initial point of the history, or
  - (b) any path used in a previous count.

Note that the maxima and minima of each stress or strain component may not happen at the beginning or at the end of the counted half-cycle, as discussed before. It may happen at any point along the cycle. Therefore, any stress or strain range must be computed considering the maximum and minimum values along the entire path between two reversions, not only the initial and final values from the half-cycle.

The following example clarifies the necessary steps to implement this routine. The objective is to rainflow count the multiaxial NP history of cyclic tension–torsion formed by successive blocks of normal and shear strains given by  $(\epsilon_x, \gamma_{xy}) = \{(2,1) \rightarrow (-1,2) \rightarrow (2,-2) \rightarrow (-2,-2) \rightarrow (2,2) \rightarrow (-2,0)\}\%$  repeatedly applied to a steel specimen.

Assuming the elastic Poisson coefficient  $\nu_{el} = 0.3$  and  $\epsilon_{el} \cong \epsilon_{pl}$ , the effective Poisson coefficient [1] is  $\bar{\nu} = (\nu_{el}\epsilon_{el} + 0.5\epsilon_{pl}) / (\epsilon_{el} + \epsilon_{pl}) = 0.4$ . Defining  $\epsilon \equiv \epsilon_x$  and  $\gamma \equiv \gamma_{xy}$ , and using Hooke's law assuming  $\sigma_y = \sigma_z = 0$ , one can obtain

$$\epsilon_y = \epsilon_z = -\bar{\nu}\epsilon \Rightarrow \epsilon_{Mises} = \sqrt{\epsilon^2 + 3[\gamma/(2 + 2\bar{\nu})]^2} \quad (3)$$

Translating the block to begin at the point with highest absolute  $\epsilon_{Mises}$  (point A = (2,2), even though points E and F have the same  $\epsilon_{Mises}$  in the time history shown in Fig. 4), the  $\gamma$ - $\epsilon$  diagram from Fig. 4 is obtained. The initial point of the first event of the rainflow count is A(2,2). The relative Mises strains with respect to A are given by

$$\epsilon_{RMises}(A) = \sqrt{(\epsilon - 2\%)^2 + 3 \cdot [(\gamma - 2\%)/(2 + 2\bar{\nu})]^2} \quad (4)$$

resulting in the relative history from Fig. 5. The count of this first event stops at point F, which has the highest  $\epsilon_{RMises}$  with respect to A, see Fig. 5. Note that in the path B-B' of Fig. 5 the value of  $\epsilon_{RMises}$  is constant, therefore in the corresponding  $\gamma$ - $\epsilon$  diagram it describes an arc of ellipse centered in A and with aspect ratio  $\sqrt{3}/[2(1 + \bar{\nu})]$ . Along the entire path A-B-B'-F, the highest value of  $\epsilon = 2\%$  takes place at point A, and the lowest  $\epsilon = -2\%$  takes place at B and F. The highest  $\gamma = 2\%$  also takes place at A, and the lowest  $\gamma = -2\%$  takes place at the entire path B'-F. In this way, according to Wang–Brown's method, in this half-cycle the absolute ranges  $\Delta\epsilon = 4\%$  and  $\Delta\gamma = 4\%$  are obtained.

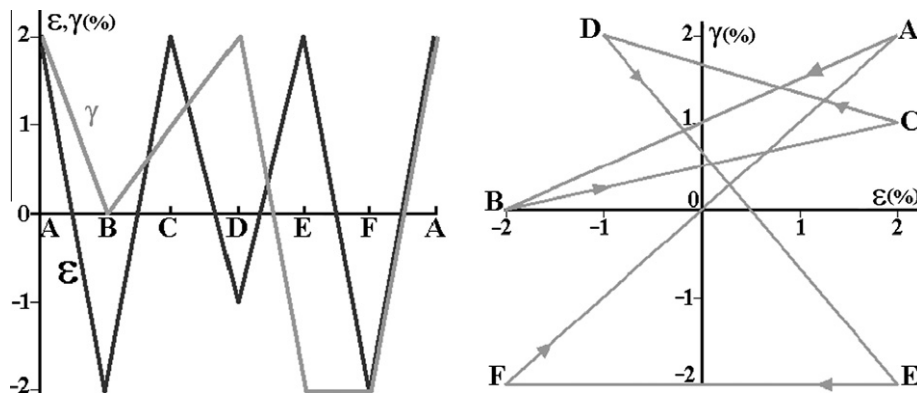


Fig. 4. Strain history for the considered NP loading and corresponding  $\gamma$ - $\epsilon$  diagram.

Note that the calculation of the exact location of point B' in the path E-F of the  $\gamma$ - $\epsilon$  diagram is important to obtain the ranges  $\Delta\epsilon$  and  $\Delta\gamma$  from the following counts. The position is calculated by finding the interpolation parameter  $\alpha$  from  $B' = (\epsilon, \gamma) = (2, -2) + \alpha \cdot [(-2, -2) - (2, -2)]$  that makes the  $\epsilon_{RMises}$  of B' with respect to A equal to 4.19% (which is equal to the  $\epsilon_{RMises}$  of point B with respect to A), hence

$$\epsilon_{RMises}(A)|_{B'} = \sqrt{[(2 - 4\alpha) - 2]^2 + 3 \left[ \frac{(-2) - 2}{2 + 2\bar{\nu}} \right]^2} = 4.19\% \quad \therefore \alpha = 0.844 \quad (5)$$

So, B' is located at  $(\epsilon, \gamma) = (2 - 4\alpha, -2) = (-1.378, -2)\%$ .

The initial point of the count of the second event is B(-2,0). The relative Mises strains with respect to B are given by

$$\epsilon_{RMises}(B) = \sqrt{(\epsilon + 2\%)^2 + 3 \cdot [(\gamma - 0\%)/(2 + 2\bar{\nu})]^2} \quad (6)$$

resulting in the relative history from Fig. 6. The count of this second event stops at point A which, together with point E, has the largest relative  $\epsilon_{RMises}$  with respect to B, see Fig. 6. The paths C-C' and E-A in the  $\gamma$ - $\epsilon$  diagram are arcs of ellipses centered at B. Note that it is important to draw the path B'-F in these two figures, to avoid counting it more than once. Note also that, if  $P_i$  is the initial point of the count, the successive plots  $\epsilon_{RMises}(P_i) \times (\text{remaining events})$  follow the rules of the traditional rainflow algorithm.

The position of point C' in the D-E path of the  $\gamma$ - $\epsilon$  diagram is interpolated by the expression  $(\epsilon, \gamma) = (-1, 2) + \alpha \cdot [(2, -2) - (-1, 2)]$ , where  $\alpha$  is the value that makes the  $\epsilon_{RMises}$  of C' with respect to B equal to 4.05% (which is equal to the  $\epsilon_{RMises}$  of C with respect to B), hence

$$\epsilon_{RMises}(B)|_{C'} = \sqrt{[(-1 + 3\alpha) - (-2)]^2 + 3 \left[ \frac{(2 - 4\alpha) - 0}{2 + 2\bar{\nu}} \right]^2} = 4.05\% \quad \therefore \alpha = 0.961 \quad (7)$$

So, C' is located at  $(\epsilon, \gamma) = (-1 + 3\alpha, 2 - 4\alpha) = (1.883, -1.844)\%$ .

Along the entire path B-C-C'-E-A, the largest value of  $\epsilon$  would be higher than 2%, taking place in the middle of the elliptic arc E-A of Fig. 6. Note, however, that the path E-A is a result of the rainflow count, it is not an actual path followed during the history. Therefore, it is reasonable to assume that the largest value of  $\epsilon$  is 2%, which happens exactly at points E and A. The minimum  $\epsilon = -2\%$  takes place in B, resulting in  $\Delta\epsilon = 4\%$  in this count according to Wang–Brown's method. The highest  $\gamma = 2\%$  takes place at A and the lowest  $\gamma = -2\%$  at E, resulting in  $\Delta\gamma = 4\%$ . Be careful not to calculate  $\Delta\gamma$  as the difference  $(2 - 0\%)$  between the values of  $\gamma$  at A and B, the final and initial points of the path, because in this case the lowest value of  $\gamma$  takes place along the path, at point E.

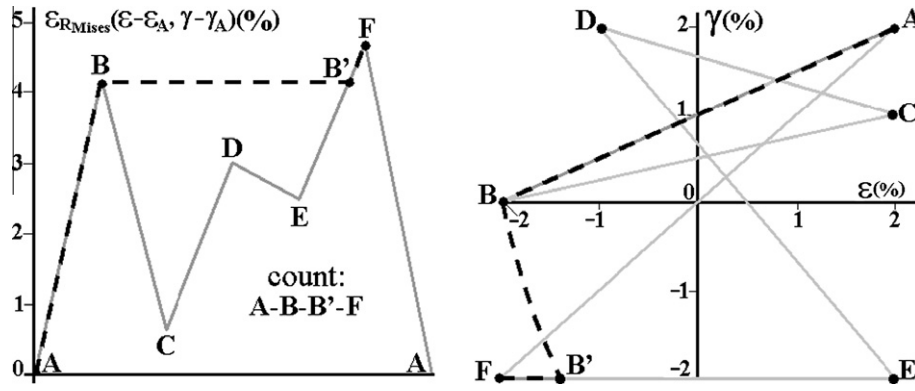


Fig. 5. Rainflow count of the first event of the history and corresponding  $\gamma$ - $\epsilon$  diagram.

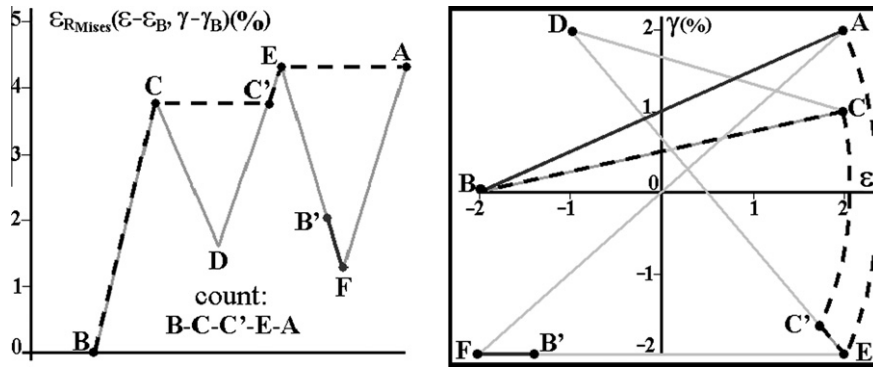


Fig. 6. Rainflow count of the second event of the history and corresponding  $\gamma$ - $\epsilon$  diagram.

A criticism to this procedure that obtains  $\Delta\gamma = 4\%$  instead of  $2\%$  is that most of the strain variation  $\Delta\epsilon$  takes place in the path B-C', whereas most of the variation  $\Delta\gamma$  takes place subsequently, in the path C-C-E-A. However, when calculating the associated damage, Wang-Brown's method assumes that both variations take place at the same time, and not sequentially. This could possibly result in conservative predictions in this case. If, on the other hand, only the extremes A and B of the path were used to calculate the strain variations, obtaining  $\Delta\gamma = 2\%$  instead of  $4\%$ , highly non-conservative predictions would be probably obtained. Such inconsistencies will be solved in the Modified Wang-Brown count proposed in the next section, where the MOI method will be used to calculate the equivalent strain (or stress) ranges associated with a complex path.

The third event begins at point C, and stops at B' because it found a previous count, as shown in Fig. 7, resulting in the path C-D-D'-B'. In the corresponding  $\gamma$ - $\epsilon$  diagram, the transition D-D' happens through an arc of ellipse centered at C, where the  $\epsilon_{RMises}$  relative to C is

$$\epsilon_{RMises}(C) = \sqrt{(\epsilon - 2\%)^2 + 3 \cdot [(\gamma - 1\%)/(2 + 2\bar{\nu})]^2} \quad (8)$$

The position of D' in the path E-F is interpolated by  $(\epsilon, \gamma) = (2, -2) + \alpha \cdot [(-2, -2) - (2, -2)]$ , where  $\alpha$  makes  $\epsilon_{RMises}$  with respect to C equal to  $3.06\%$  (the same value as  $\epsilon_{RMises}$  of D with respect to C), hence

$$\begin{aligned} \epsilon_{RMises}(C)|_{D'} &= \sqrt{[(2 - 4\alpha) - 2]^2 + 3 \left[ \frac{(-2) - 1}{2 + 2\bar{\nu}} \right]^2} = 3.06\% \quad \therefore \alpha \\ &= 0.609 \end{aligned} \quad (9)$$

So, D' is located at  $(\epsilon, \gamma) = (2 - 4\alpha, -2) = (-0.437, -2)$ .

Note that along the path C-D-D'-B' the largest  $\Delta\epsilon$  takes place between B' and C, giving a normal strain range

$\Delta\epsilon = 2\% - (-1.378\%) = 3.378\%$ , whereas the largest shear strain range  $\Delta\gamma$  takes place between the path D'-B' and point D, with  $\Delta\gamma = 2\% - (-2\%) = 4\%$ .

The counting procedure for the remaining half-cycles of the block is similar, see Figs. 8–10, resulting in the half-cycles D-C, with normal and shear strain ranges  $\Delta\epsilon = 1.883\% - (-1\%) = 2.883\%$  and  $\Delta\gamma = 2\% - (-1.844\%) = 3.844\%$ ; E-D', with  $\Delta\epsilon = 2\% - (-0.437\%) = 2.437\%$  and  $\Delta\gamma = 0\%$ ; and F-A, with  $\Delta\epsilon = 4\%$  and  $\Delta\gamma = 4\%$ , according to Wang-Brown's algorithm.

The multiaxial rainflow count results in the ranges and mean loads shown in Fig. 11, corresponding to the paths A-B-B'-F, B-C-C'-E-A, C-D-D'-B', D-C, E-D' and F-A, represented by arrows in the  $\gamma$ - $\epsilon$  diagram.

Multiaxial damage models based on strain ranges, e.g. Brown-Miller, Fatemi-Socie or SWT, can then be applied to these half-cycles. Note that the Sines and Findley models are not applicable in this case, because  $\epsilon_a$  and/or  $\gamma_a \geq 2\%$  implies in significant plasticity for metals, while those models assume linear elastic strains; besides, Sines' model should not be used in NP histories.

### 5. Modified Wang-Brown (MWB) algorithm

The original Wang-Brown algorithm is not difficult to be implemented in histories of uniaxial tension/bending combined with torsion, which can be represented only by one normal  $\sigma_x$  and one shear  $\tau_{xy}$  stress components (or one normal  $\epsilon_x$  and one shear  $\gamma_{xy}$  strain components). In this case, the sub-space of normal and shear components is planar (it is represented by a diagram in only two dimensions), and the only difficulty in applying the algorithm happens when solving for the equations of the ellipses associated with the points with same relative Mises stress or strain.

However, in a generic multiaxial history, the dimension of the diagram may be increased, requiring the calculation of

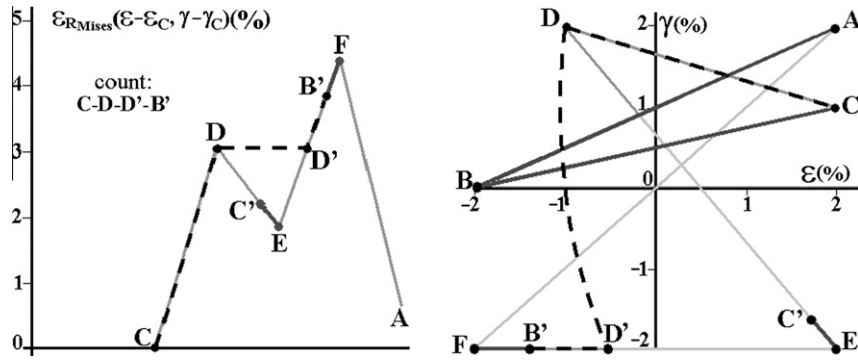


Fig. 7. Rainflow count of the third event of the history and corresponding  $\gamma$ - $\varepsilon$  diagram.

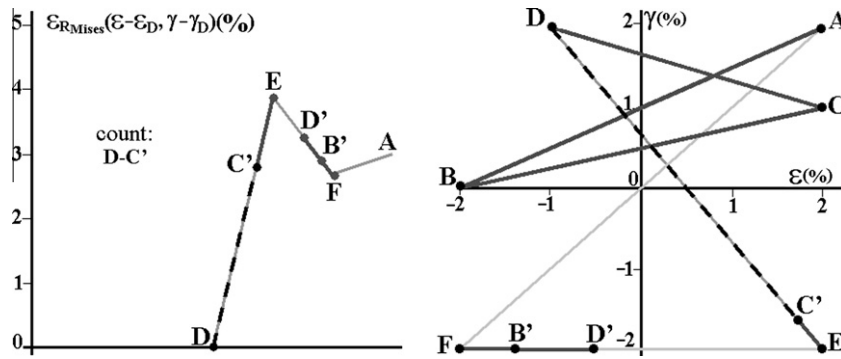


Fig. 8. Rainflow count of the fourth event of the history and corresponding  $\gamma$ - $\varepsilon$  diagram.

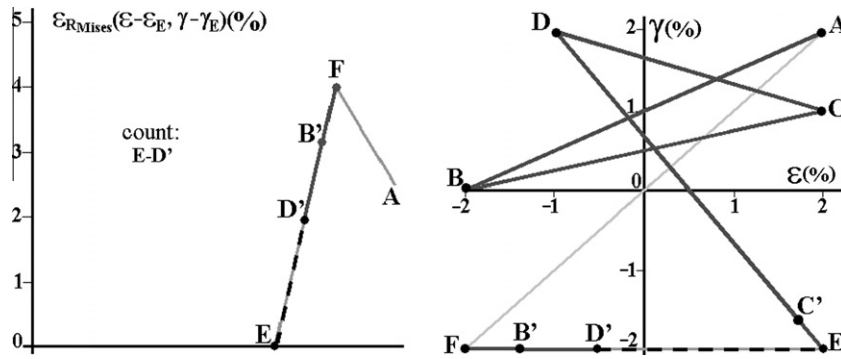


Fig. 9. Rainflow count of the fifth event of the history and corresponding  $\gamma$ - $\varepsilon$  diagram.

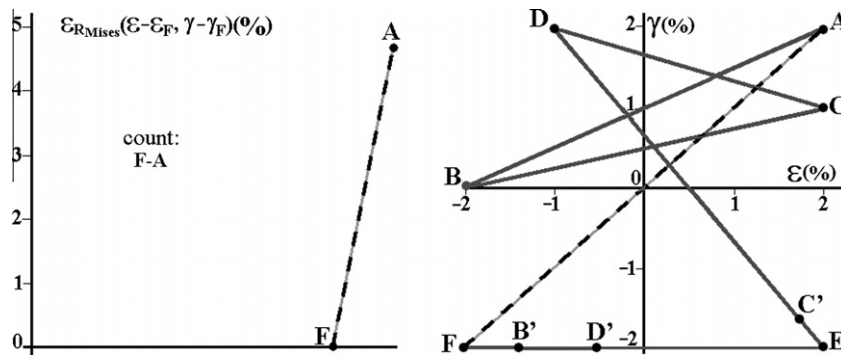


Fig. 10. Rainflow count of the last event of the history and corresponding  $\gamma$ - $\varepsilon$  diagram.

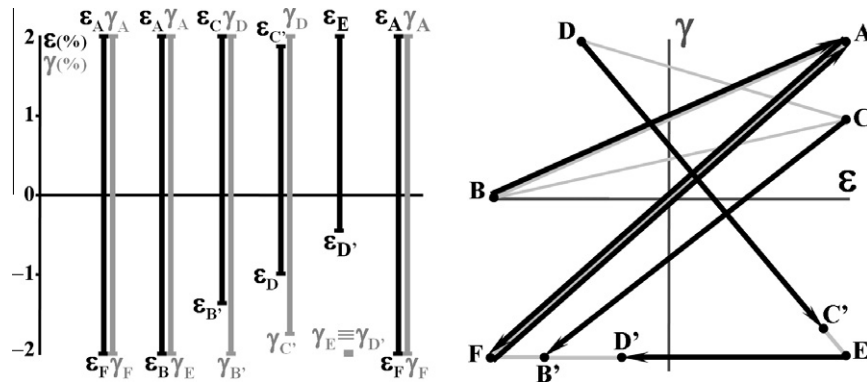


Fig. 11. Rainflow-counted strain ranges and corresponding  $\gamma$ - $\epsilon$  diagram with arrows representing the resulting half-cycles.

intersections between straight lines and ellipsoid or hyper-ellipsoid surfaces, increasing the computational complexity.

The Modified Wang–Brown method solves this problem by working in the reduced five-dimensional stress  $E_{5\sigma}$  [6] or strain  $E_{5\epsilon}$  sub-spaces presented in Part I of this paper, or in a lower dimension sub-space from them. In this way, a general multiaxial strain or stress history is represented by a set of points  $P_i = (e_1, e_2, e_3, e_4, e_5)$  or  $P_i = (S_1, S_2, S_3, S_4, S_5)$ , respectively, where

$$S_1 \equiv \sigma_x - \frac{\sigma_y}{2} - \frac{\sigma_z}{2} = \frac{3}{2}S_x, \quad S_2 \equiv \frac{\sigma_y - \sigma_z}{2} \sqrt{3} = \frac{S_y - S_z}{2} \sqrt{3} \quad (10)$$

$$S_3 \equiv \tau_{xy} \sqrt{3}, \quad S_4 \equiv \tau_{xz} \sqrt{3}, \quad S_5 \equiv \tau_{yz} \sqrt{3}$$

$$e_1 \equiv \frac{3}{2} \cdot \frac{e_x}{1 + \bar{\nu}} = \frac{2e_x - e_y - e_z}{2 \cdot (1 + \bar{\nu})}, \quad e_2 \equiv \frac{e_y - e_z}{2 \cdot (1 + \bar{\nu})} \sqrt{3} = \frac{e_y - e_z}{2 \cdot (1 + \bar{\nu})} \sqrt{3},$$

$$e_3 \equiv \frac{\gamma_{xy} \sqrt{3}}{2 \cdot (1 + \bar{\nu})}, \quad e_4 \equiv \frac{\gamma_{xz} \sqrt{3}}{2 \cdot (1 + \bar{\nu})}, \quad e_5 \equiv \frac{\gamma_{yz} \sqrt{3}}{2 \cdot (1 + \bar{\nu})} \quad (11)$$

Wang–Brown’s multiaxial rainflow algorithm is rather simplified when working in such spaces, because the distance between two points is already the relative Mises strain (or stress) between them. The three rules of the rainflow count have now simple geometric interpretations, resulting in:

1. The count must be initiated at the point with highest norm, i.e., with the longest Euclidean distance to the origin of the diagram. This first initial counting point is called  $P_1$ , and the subsequent ones are called  $P_2, \dots, P_n$ , in the same sequence of the original history.
2. Each count must be sequentially initiated at each point  $P_i$  of the diagram.
3. The final point of each count is obtained when reaching:
  - (a) the point  $P_j$  most distant from the initial point  $P_i$  (with  $j > i$ ) in the reduced sub-space, or
  - (b) any path used in a previous count.

The first rule in Wang–Brown’s algorithm was conceived to try to guarantee that the largest  $\epsilon_{RMises}$  (or relative Mises stress  $\sigma_{RMises}$ ) of the history is identified, one of the main objectives of a rainflow count. However, this rule can fail to reach this objective if the point  $P_1$  with largest norm is not one of two points of the diagram farthest apart from each other.

This is easy to check in the example from Fig. 12, which shows an  $e_1$ - $e_3$  strain diagram with a triangular path. The point  $(e_1, e_3) = (0.8\%, 0\%)$  is clearly the one with largest norm, equal to 0.8%, however its Wang–Brown count results in two half-cycles with  $\epsilon_{RMises} = 1.0\%$ . Instead, if the count was started at the point  $(e_1, e_3) = (0\%, 0.6\%)$ , both half-cycles would result in  $\epsilon_{RMises} = 1.1\%$ .

It is not difficult to prove that the largest relative Mises strain (or stress) of the history can be underestimated by up to  $1 - \sqrt{2}/2 = 29.3\%$  using the original Wang–Brown algorithm. Even if an enclosing surface method or the MOI method were applied to the resulting half-cycles, to account for the shape of the entire path, and not only the value of  $\epsilon_{RMises}$ , the original Wang–Brown algorithm would still underestimate the resulting equivalent ranges. The conclusion is that the starting point of the first count must be better chosen.

So, the first rule of the multiaxial rainflow count is now modified. The modified rule is to search for the pair of points in the deviatoric space with largest relative distance, and between them the point  $P_1$  farthest from the origin. But the Modified Wang–Brown (MWB) algorithm differs from the original method not only in such first rule. Other rules are modified and introduced as well. The MWB method can be summarized by a set of 8 rules:

1. Find among the  $n \cdot (n - 1)/2$  pairs of points from an  $n$ -point path the one(s) that form the longest chord in the 5D strain (or stress) sub-space, and choose among them the one with greatest distance from the origin; label this point  $P_1$ , and the subsequent  $P_2, \dots, P_n$  following their original order.
2. Each count should be sequentially initiated at  $P_1, P_2, \dots, P_i, \dots, P_n$ .
3. The final point in each count is obtained when reaching:
  - (a) the point  $P_j$  farthest away (in an Euclidian sense) from the initial point  $P_i$  ( $j > i$ ), or
  - (b) any finite segment (not just a point or a finite number of points) from a previous count;
4. Once found the initial and final points  $P_i$  and  $P_j$ , the count is defined by the traveled path portions closest to the straight segment  $P_i$ - $P_j$  in an Euclidean sense (to avoid long “detours” from the straight line  $P_i$ - $P_j$  that defines such half-cycle).

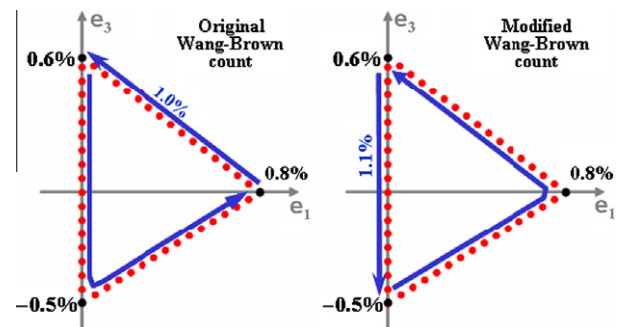


Fig. 12. Rainflow counts using the original Wang–Brown algorithm (left) and the modified version (right) for a triangular path.

5. Every time a full cycle is counted, i.e. two half-cycles with identical extreme points are counted, use the Moment Of Inertia (MOI) method (or some enclosing surface method) to calculate the equivalent strain (or stress) range and mean or maximum from the full cycle to obtain the associated fatigue damage using some multiaxial model.
6. After rainflow counting the entire load history, repeat step 5 to calculate the damage contribution of the half-cycles that did not close into a full cycle.
7. Use some damage accumulation rule, e.g., Miner's rule [25], to find the total multiaxial damage.
8. If using a critical plane approach, repeat steps 1–7 for every candidate plane, to find the critical plane that maximizes the accumulated multiaxial damage; note that only Case B candidate planes will need a multiaxial rainflow count, because the single shear component in Case A cracks can be counted using a uniaxial rainflow algorithm such as the one in [15].

Note that the Moment Of Inertia (MOI) method, presented in Part I of this paper, finds a better estimate of the equivalent range associated with a counted cycle or half-cycle, better than simply searching for the extreme values of each component along the path, as the original Wang–Brown method did. The original method would combine ranges in different components that did not happen at the same time, losing information about the degree of non-proportionality of the counted path and the phase difference between components.

### 6. Computational implementation of the MWB algorithm

The practical implementation of the proposed MWB multiaxial rainflow count is described next, including a detailed description of its computational algorithm. During the execution of the algorithm, when a segment  $P_i-P_{i+1}$  is counted, totally or partially, an interpolation variable  $\alpha_i$  ( $1 \leq i \leq n$ ) is associated to it, such that  $0 \leq \alpha_i \leq 1$ . If the entire segment  $P_i-P_{i+1}$  has been counted, then  $\alpha_i = 0$ , otherwise  $\alpha_i$  is computed from the intersection  $P'_i$  between  $P_i-P_{i+1}$  and the most recent count, see Fig. 13, using

$$\alpha_i = \frac{|P'_i - P_i|}{|P_{i+1} - P_i|} \quad (12)$$

In this way, a segment associated with  $0 < \alpha_i < 1$  will have its segment  $P'_i - P_{i+1}$  already counted, whereas the portion  $P_i - P'_i$  is still available for future counts, where  $P'_i = P_i + \alpha_i \cdot (P_{i+1} - P_i)$ .

In the computational algorithm, all  $\alpha_i$  are initialized with some value outside the interval  $[0, 1]$  (e.g.  $\alpha_i = -1$ , for  $i = 1, 2, \dots, n$ ) to indicate that, initially, no path has been counted. Note that it is possible to have  $\alpha_i = 1.0$  if a previous count crossed the segment exactly at  $P_{i+1}$ , which would create a stopping point for future counts, but without using up any portion of the segment  $P_i - P_{i+1}$ . But rule 3 above states that a point or a finite number of points previously counted cannot define the end of a count, therefore any  $\alpha_i = 1.0$  must be reset to  $\alpha_i = -1$  in the algorithm not to create a

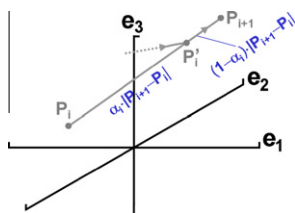


Fig. 13. Definition of the variable  $\alpha_i$  that delimits the segment  $P'_i - P_{i+1}$  already accounted for and the segment  $P_i - P'_i$  that will still be counted by the MWB algorithm.

stopping point at  $P_{i+1}$  in this case. Note that in the algorithm the history paths are all assumed as formed by straight segments. If however the paths are curved, then they must be approximated by sufficiently refined polygonal paths.

Since the transformations that converted the stress and strain components into their deviatoric forms, as well as the transformations that projected them onto the reduced sub-spaces  $E_{5\sigma}$  and  $E_{5\epsilon}$ , are all linear (even for the elastoplastic case), the stresses and strains at a point  $P'_i$  in the straight segment  $P_i - P_{i+1}$  can be linearly calculated from  $\alpha_i$  and the coordinates of points  $P_i$  and  $P_{i+1}$ . E.g., the projected deviatoric strain  $e_1$  at point  $P'_i$  is simply  $\epsilon_{1,i} + \alpha_i \cdot (\epsilon_{1,(i+1)} - \epsilon_{1,i})$ . This linearity simplifies very much the calculations in the proposed multiaxial rainflow algorithm, eliminating the need to calculate intersections between segments and ellipses, ellipsoids or hyper-ellipsoids, as it was required in the original Wang–Brown algorithm.

As mentioned before, the multiaxial rainflow count starts at each point  $P_i$  of the history,  $i = 1, 2, \dots, n$ . The algorithm to perform the count from an initial point  $P_i$  is described next.

If the path  $P_i - P_{i+1}$  is already associated with a variable  $\alpha_i$  different than  $-1$ , calculated during a previous count, then the count stops, and the stopping point will be  $P'_i = P_i + \alpha_i \cdot (P_{i+1} - P_i)$ . Otherwise, if the path  $P_i - P_{i+1}$  is not associated with any  $\alpha_i$  different than  $-1$ , then this entire segment is counted and  $\alpha_i$  is set to zero.

Next, the algorithm searches for the first point  $P_{j+1}$  ( $j > i$ ) that has a greater or equal distance to  $P_{i+1}$  with respect to  $P_i$ . If it does not exist, then  $P_{i+1}$  will be the final point of the count. Otherwise, the intersection with the segment  $P_j - P_{j+1}$  is calculated at the point  $P'_j$  with same distance to point  $P_i$  as  $P_{i+1}$ , see Fig. 14. The value of  $\alpha_j$  associated with point  $P'_j$  is obtained from Stewart's Theorem [27] applied to triangle  $P_i - P_j - P_{j+1}$

$$b^2 \cdot [(1 - \alpha_j) \cdot a] + c^2 \cdot [\alpha_j \cdot a] - p^2 \cdot a = [\alpha_j \cdot a] \cdot [(1 - \alpha_j) \cdot a] \cdot a \quad (13)$$

where  $b$ ,  $c$  and  $p$  are defined in Fig. 14, resulting in

$$a^2 \cdot \alpha_j^2 + (c^2 - b^2 - a^2) \cdot \alpha_j + (b^2 - p^2) = 0 \quad (14)$$

$$\alpha_j = \frac{(a^2 + b^2 - c^2) \pm \sqrt{(a^2 + b^2 - c^2)^2 - 4a^2(b^2 - p^2)}}{2a^2} \quad (15)$$

The valid solution will be the lowest  $\alpha_j = \alpha'_j$  (between the 2 solutions) that satisfies  $0 \leq \alpha'_j \leq 1$ . If the segment  $P_j - P_{j+1}$  was already associated with some  $\alpha_j = \alpha_j^*$  (i.e., a portion from it had already been counted), then there are two hypotheses: (i) if  $\alpha'_j < \alpha_j^*$ , then the portion between  $\alpha'_j$  and  $\alpha_j^*$  is counted, the stopping point becomes the one associated with  $\alpha'_j$  (since it crossed a segment from a previous count), and  $\alpha_j = \alpha'_j$  is stored, replacing  $\alpha_j^*$ ; or (ii) if  $\alpha'_j \geq \alpha_j^*$ , then the intersection point  $P'_j$  would be invalid since it would take place on a previously counted segment, therefore the stopping point must be set as  $P_{i+1}$ .

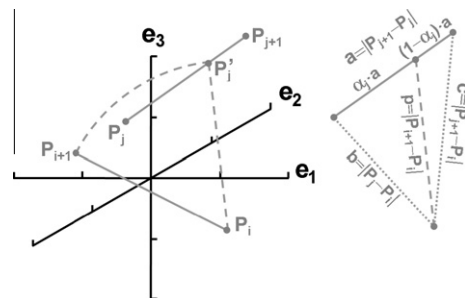


Fig. 14. Calculation of the intersection point  $P'_j$  between the current multiaxial rainflow count and the segment  $P_j - P_{j+1}$  in a sub-space of  $E_{5\epsilon}$  (or  $E_{5\sigma}$ ). Note that, usually, the triangles  $P_i - P_j - P_{j+1}$  and  $P_i - P_{i+1} - P'_j$  do not share the same plane.

On the other hand, if no portion of the segment  $P_j-P_{j+1}$  had been accounted for (i.e.,  $\alpha_j$  was equal to  $-1$ ), then the calculated  $\alpha'_j$  is stored in  $\alpha_j$ , counting then the segment  $P'_j-P_{j+1}$ . As mentioned before, if  $\alpha_j$  results in 1.0 then it must be reset to  $\alpha_j = -1$  not to create an unnecessary stopping point for future counts. This count continues from  $P_{j+1}$  in a similar way as the one coming from  $P_{i+1}$ . The algorithm then searches for the first point  $P_{m+1}$  ( $m > j$ ) with a greater or equal distance than  $P_{j+1}$  with respect to  $P_i$ . If it does not exist, then  $P_{j+1}$  will be the final point of this count. Otherwise, the intersection with the segment  $P_m-P_{m+1}$  is calculated at a point  $P'_m$ , with the same distance as  $P_{j+1}$  with respect to  $P_i$ . The value of  $\alpha'_m = \alpha'_m$  associated with  $P'_m$  is obtained applying Stewart's Theorem [27] to the triangle  $P_i-P_m-P_{m+1}$ . The expression of  $\alpha'_m$  is analogous to the one obtained before for  $\alpha_j$ , being enough to exchange  $P_j$  for  $P_m$ ,  $P_{j+1}$  for  $P_{m+1}$ , and  $P_{i+1}$  for  $P_{j+1}$ .

The above procedure continues in a similar way. If the segment  $P_m-P_{m+1}$  was already associated to some  $\alpha'_m = \alpha'_m$  different than  $-1$ , then there are 2 hypotheses: (i) if  $\alpha'_m < \alpha'_m$ , then the segment bounded by the points associated with  $\alpha'_m$  and  $\alpha'_m$  is counted, the stopping point is associated with  $\alpha'_m$ , and  $\alpha_m = \alpha'_m$  is stored, replacing  $\alpha'_m$ ; or (ii) if  $\alpha'_m \geq \alpha'_m$ , then the intersection point  $P'_m$  would be invalid and the stopping point is  $P_{j+1}$ . If no portion of the path  $P_m-P_{m+1}$  had been counted, then the value  $\alpha_m = \alpha'_m$  is stored, the seg-

ment  $P'_m-P_{m+1}$  is counted, and the count continues from  $P_{m+1}$ . The algorithm then searches for the first point  $P_{r+1}$  ( $r > m$ ) with a longer distance than  $P_{m+1}$  with respect to  $P_i$ , and so on.

The algorithm continues until the stopping point for the count started at  $P_i$  is found. The linearity of the adopted transformations allows all resulting stresses and strains at any intersection point to be obtained from a simple interpolation involving the  $\alpha_i$  coefficients.

The entire process is performed for all starting points  $P_i$  ( $i = 1, 2, \dots, n$ ). Note that a count can stop at point  $P_i$  if the history is periodic, in which case the segment  $P_n-P_1$  exists and it cannot be left out. At the end of the algorithm, all segments will be associated with values  $\alpha_i = 0$ , indicating that all of them were entirely counted. Fig. 15 shows the flowchart of the entire MWB algorithm.

## 7. Application of the MWB algorithm

In this section, the MWB rainflow algorithm is applied to the NP history presented in Section 4, formed by blocks of  $(\varepsilon_x, \gamma_{xy}) = \{(2, 1) \rightarrow (-1, 2) \rightarrow (2, -2) \rightarrow (-2, -2) \rightarrow (2, 2) \rightarrow (-2, 0)\}$  repeatedly applied to a steel specimen. This step-by-step example is important to point out several implementation details of the algorithm.

Assuming  $\nu_{el} = 0.3$  and  $\varepsilon_{el} \cong \varepsilon_{pl}$ , it is found that  $\bar{\nu} = 0.4$ . Defining  $\varepsilon \equiv \varepsilon_x$  and  $\gamma \equiv \gamma_{xy}$ , and using Hooke's law assuming  $\sigma_y = \sigma_z = 0$ , then  $\varepsilon_y = \varepsilon_z = -\bar{\nu}\varepsilon$ . The projection onto the  $E_{5e}$  sub-space results in

$$\begin{aligned} e_1 &= \frac{2\varepsilon_x + \bar{\nu}\varepsilon_x + \bar{\nu}\varepsilon_x}{2 \cdot (1 + \bar{\nu})} = \varepsilon_x, & e_2 &= \frac{\varepsilon_y - \varepsilon_z}{2 \cdot (1 + \bar{\nu})} \sqrt{3} = 0, \\ e_3 &= \frac{\gamma_{xy} \sqrt{3}}{2 \cdot (1 + \bar{\nu})}, & e_4 &= 0, e_5 = 0 \end{aligned} \quad (16)$$

which can be represented in the 2D sub-space.  $\bar{e}''' \equiv [e_1 e_3]^T$ . The projected history is then given by  $(e_1, e_3) = (\varepsilon_x, 0.6186 \cdot \gamma_{xy}) = \{(2, 0.6186) \rightarrow (-1, 1.2372) \rightarrow (2, -1.2372) \rightarrow (-2, -1.2372) \rightarrow (2, 1.2372) \rightarrow (-2, 0)\}$ %. Among all pairs of points (consecutive or not) of the history, the most distant pair (i.e., with the highest  $\varepsilon_{RMises}$  between them) is  $(-2, -1.2372)\%$  and  $(2, 1.2372)\%$ , called F and A, respectively, in the example from Section 4, see Fig. 16. The distance between them in the 2D deviatoric sub-space is  $\varepsilon_{RMises} = 4.7035\%$ . Since both points have the same distance 2.3517% to the origin, any of the two can be chosen to be the first initial point  $P_1$ . Choosing the point  $(2, 1.2372)\%$  (previously called A) to be  $P_1$ , the subsequent points are called  $P_2, P_3, P_4, P_5$  and  $P_6$  (B, C, D, E and F, respectively, in the example from Section 4), following the same order of the original cyclic history, see Fig. 16. This periodic history, re-ordered starting from  $P_1$ , becomes then  $(e_1, e_3) = \{(2, 1.2372) \rightarrow (-2, 0) \rightarrow (2, 0.6186) \rightarrow (-1, 1.2372) \rightarrow (2, -1.2372) \rightarrow (-2, -1.2372)\}$ %.

The count that begins in  $P_1$  uses up the entire segment  $P_1-P_2$ , resulting in  $\alpha_1 = 0$ . It is easy to see in Fig. 16 that the only point more distant than  $P_2$  with respect to  $P_1$  is  $P_6$ , therefore  $a = |P_6 - P_5| = 4.0\%$ ,  $b = |P_5 - P_1| = 2.4744\%$ ,  $c = |P_6 - P_1| = 4.7035\%$  and  $p = |P_2 - P_1| = 4.1870\%$ , resulting in

$$\begin{aligned} \alpha_5 &= \frac{(a^2 + b^2 - c^2) \pm \sqrt{(a^2 + b^2 - c^2)^2 - 4a^2(b^2 - p^2)}}{2a^2} \\ &= \begin{cases} 0.8444 \\ -0.8444 \end{cases} \end{aligned} \quad (17)$$

The lowest solution above that satisfies  $0 \leq \alpha_5 \leq 1$  is  $\alpha_5 = 0.8444$ . The first count then ends at point  $P_6$ , the most distant from  $P_1$ , resulting in the path  $P_1-P_2-P'_5-P_6$ , where  $P'_5 = P_5 + \alpha_5 \cdot (P_6 - P_5) = (-1.3776, -1.2372)\%$ . Note that  $P'_5$  corresponds to point B' from the example from Section 4, as expected.

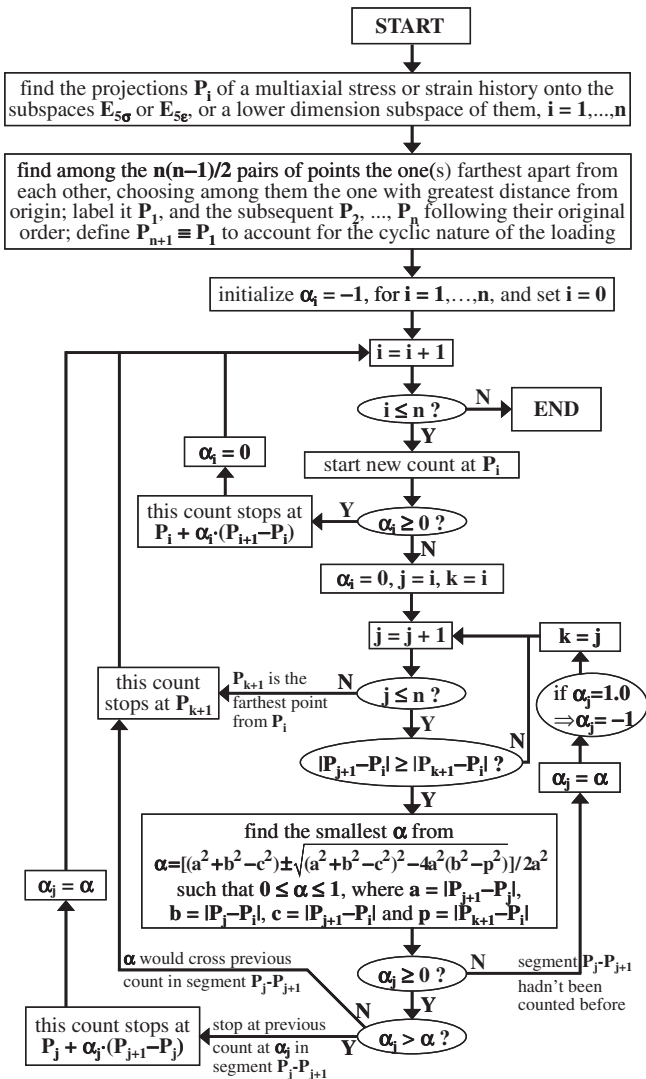


Fig. 15. Flowchart of the proposed Modified Wang-Brown (MWB) algorithm.

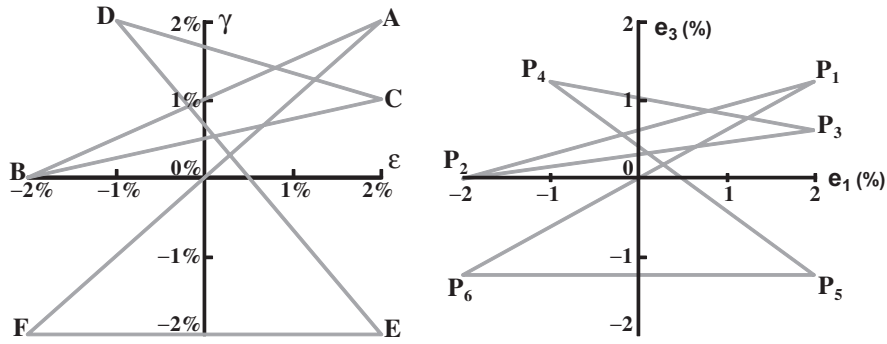


Fig. 16.  $\gamma$ - $\varepsilon$  diagram of the considered NP history and corresponding path in a deviatoric subspace.

The count that begins in  $P_2$  uses up the entire segment  $P_2$ - $P_3$ , resulting in  $\alpha_2 = 0$ . The next point more distant than  $P_3$  with respect to  $P_2$  is  $P_5$ , hence  $a = |P_5 - P_4| = 3.8888\%$ ,  $b = |P_4 - P_2| = 1.5908\%$ ,  $c = |P_5 - P_2| = 4.1870\%$ , and  $p = |P_3 - P_2| = 4.0475\%$ , resulting in  $\alpha_4 = 0.9611$  or  $-0.9530$ . The lowest solution that satisfies  $0 \leq \alpha_4 \leq 1$  is  $\alpha_4 = 0.9611$ . The count then reaches point  $P_5$ , but since  $P_1$  (which would be called  $P_{n+1} = P_{6+1} = P_7$  according to the algorithm of Fig. 15) and  $P_5$  have the same distance 4.1870% with respect to  $P_2$ , then the condition  $|P_7 - P_2| |P_5 - P_2|$  is true, and so the count continues, only stopping in  $P_7 \equiv P_1$ , the most distant point from  $P_2$ . Since this count arrived at  $P_1$  without going through the segment  $P_6$ - $P_1$ ,  $\alpha_6$  becomes equal to 1.0. To avoid creating an unnecessary stopping point for future counts at the end of  $P_6$ - $P_1$  due to  $\alpha_6 = 1.0$ , the algorithm resets  $\alpha_6 = -1$ . In summary, this second count results in the path  $P_2$ - $P_3$ - $P'_4$ - $P_5$ - $P'_6$ , where  $P'_4 = P_4 + \alpha_4 \cdot (P_5 - P_4) = (1.8834, -1.1410)\%$ , and  $P'_6 = P_6 + \alpha_6 \cdot (P_7 - P_6) \equiv P_7 \equiv P_1$ .  $+ \alpha_6 \cdot (P_7 - P_6) \equiv P_7 \equiv P_1$ . Note that this path corresponds to B-C-E-A from the example from Section 4, as expected.

The count that begins in  $P_3$  uses up the entire segment  $P_3$ - $P_4$ , thus  $\alpha_3 = 0$ . The next point more distant than  $P_4$  with respect to  $P_3$  is  $P_6$ , so  $a = |P_6 - P_5| = 4.0\%$ ,  $b = |P_5 - P_3| = 1.8558\%$ ,  $c = |P_6 - P_3| = 4.4095\%$  and  $p = |P_4 - P_3| = 3.0631\%$ , obtaining  $\alpha_5 = 0.6092$  or  $-0.6092$ , hence  $\alpha_5 = 0.6092$ . However, a previous count had already used part of the segment  $P_5$  -  $P_6$ , with an intersection point  $P'_5$  associated with  $\alpha_5 = 0.8444$ . Since  $0.6092 < 0.8444$ , the value of  $\alpha_5$  is updated with  $\alpha_5 = 0.6092$ , a new intersection point before  $P'_5$  is defined in the segment  $P_5$ - $P_6$ , denominated  $P''_5 = P_5 + \alpha_5 \cdot (P_6 - P_5) = (-0.4370, -1.2372)\%$ , and this count stops at  $P''_5$  since it reaches a segment  $P'_5$ - $P_6$  used in a previous count. The resulting path is then  $P_3$ - $P_4$ - $P''_5$ - $P'_6$ , which corresponds to C-D-D'-B' from the example from Section 4.

The count that begins in  $P_4$  needs to stop at point  $P'_4$ , associated with  $\alpha_4 = 0.9611$ , because the portion  $P'_4$ - $P_5$  had already been counted. The resulting path is then  $P_4$ - $P'_4$  and  $\alpha_4$  is set to zero. Similarly, the count that begins in  $P_5$  needs to stop at point  $P'_5$ , associated with  $\alpha_5 = 0.6092$ , because the portion  $P'_5$ - $P_5$ - $P_6$  had already been counted. The resulting path is  $P_5$ - $P'_5$  and  $\alpha_5$  is set to zero.

Finally, the count that begins in  $P_6$  needs to stop at its most distant point  $P_7 \equiv P_1$ . Note that  $P'_6$  itself did not constitute a stopping point because it was the single point of the segment  $P_6$ - $P_7$  used in previous counts. Only previously counted segments (and not points or finite sets of points) can stop a count before reaching the most distant point, this is why  $\alpha_6$  had been reset to  $-1$ , instead of leaving its previously calculated value 1.0. The resulting counted path is  $P_6$ - $P_1$  and  $\alpha_6$  is set to zero.

When the algorithm ends, the entire history has been accounted for, and all  $\alpha_i$  end up with zero values, as expected. The MWB count results in this example in the exact same half-cycles from the original Wang-Brown method obtained in the example from Section 4, see Fig. 17, however with a much lower complexity and

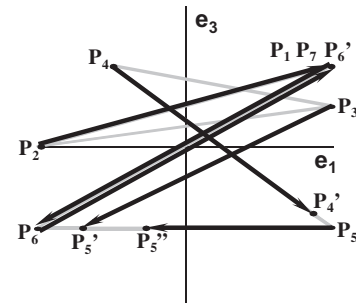


Fig. 17. MWB count in a deviatoric strain sub-space, with arrows representing the resulting half-cycles.

computational cost. The MWB algorithm has simple geometric interpretations, it does not require the calculation of intersections with hyperellipses, and it does not require the recalculation of all  $\varepsilon_{RMises}$  for every count. In addition, it always finds the events with largest  $\varepsilon_{RMises}$ , as opposed to the traditional Wang-Brown method, as discussed before.

To calculate the fatigue damage, the MWB method first tries to combine half-cycles into full cycles, and then it applies the MOI method to calculate the equivalent strain (or stress) ranges associated with each count. Using the MOI (or even an enclosing surface) method is a considerable improvement over the original Wang-Brown method, which defined the ranges of each component only from their maxima and minima along the path, losing information about non-proportionality and phase difference between the components.

In this example, the MOI method would be applied to the half-cycles defined by the paths  $P_4$ - $P'_4$ ,  $P_5$ - $P'_5$ ,  $P_3$ - $P_4$ - $P''_5$ - $P'_6$  and  $P_2$ - $P_3$ - $P'_4$ - $P_5$ - $P'_6$ , and to the combined full cycle  $P_1$ - $P_2$ - $P'_5$ - $P_6$ - $P_7$ . Note that these paths are presented above ordered by the last point of each path, to try to preserve load order information, similarly to the sequential rainflow algorithm [23–24]. This reordering is simple to implement computationally, and it is very important for very long non-periodic histories, in special in the presence of plastic strains (due to plasticity memory effects).

After obtaining the equivalent ranges and mean components of all rainflow-counted paths, any multiaxial model can be applied to calculate the accumulated damage at the considered candidate plane. The critical plane will then be the candidate plane with highest accumulated damage, as discussed before.

### 8. Conclusions

Wang and Brown proposed a multiaxial rainflow count based on the relative Mises strain  $\varepsilon_{RMises}$  as an indirect measure of the

damage during a half-cycle. But the original method requires the calculation of  $\epsilon_{RMises}$  at every rainflow count for all subsequent starting points. In this work, a Modified Wang–Brown (MWB) rainflow counting method was proposed, based on the representation of the stress or strain history in a reduced 5D sub-space of the six deviatoric strain (or stress) components. The MWB uses improved rules to guarantee that the event with highest  $\epsilon_{RMises}$  is always counted. The MWB method can be applied to a critical plane approach to range-count the two shear components present in Case B cracks, using a 2D sub-space of the considered 5D deviatoric space. Coupled with the Moment Of Inertia or some enclosing surface method, the MWB can better account for the path shape influence on the associated fatigue damage. The method has simple geometric interpretations that considerably simplify its implementation: e.g. the distance between 2 points in the considered deviatoric strain sub-space is the  $\epsilon_{RMises}$  between them. The computational implementation of the algorithm was discussed in detail, including a detailed flowchart with all necessary calculation steps.

## References

- [1] Socie DF, Marquis GB. Multiaxial fatigue; 1999.
- [2] Deperrois A. Sur le calcul des limites d'endurance des aciers Thèse de Doctorat. Paris: Ecole Polytechnique; 1991.
- [3] Kida S, Itoh T, Sakane M, Ohnami M, Socie DF. Dislocation structure and non-proportional hardening of type 304 stainless steel. *Fatigue Fract Eng Mater Struct* 1997;20(10):1375–86.
- [4] Shamsaei N, Fatemi A, Socie DF. Multiaxial cyclic deformation and non-proportional hardening employing discriminating load paths. *Int J Plast* 2010;26(12):1680–701.
- [5] Wang CH, Brown MW. Life prediction techniques for variable amplitude multiaxial fatigue – Part 1: Theories. *J Eng Mater Technol* 1996;118:pp-370.
- [6] Papadopoulos IV, Davoli P, Gorla C, Fillippini M, Bernasconi A. A comparative study of multiaxial high-cycle fatigue criteria for metals. *Int J Fatigue* 1997;19(3):219–35.
- [7] Sines G. Behavior of metals under complex static and alternating stresses. *Metal fatigue*. McGraw-Hill; 1959. pp. 145–69.
- [8] Crossland B. Effect of large hydrostatic pressures on the torsional fatigue strength of an alloy steel. In: Proceedings of international conference on fatigue of metals. London: Springer; 1956. p. 138–49.
- [9] Findley WN. A theory for the effect of mean stress on fatigue of metals under combined torsion and axial load or bending. *J Eng Ind* 1959;301–6.
- [10] McDiarmid DL. A general criterion for high cycle multiaxial fatigue failure. *Fatigue Fract Eng Mater Struct* 1991;14(4):429–53.
- [11] McDiarmid DL. A shear stress based critical-plane criterion of multiaxial fatigue failure for design and life prediction. *Fatigue Fract Eng Mater Struct* 1994;17(12):1475–85.
- [12] Brown M, Miller KJ. A theory for fatigue under multiaxial stress–strain conditions. *Inst Mech Eng* 1973;187:pp-756.
- [13] Fatemi A, Socie DF. A critical plane approach to multiaxial damage including out-of-phase loading. *Fatigue Fract Eng Mater Struct* 1988;11:149–66.
- [14] Smith RN, Watson P, Topper TH. A stress–strain parameter for the fatigue of metals. *J Mater* 1970;5(4):767–78.
- [15] Langlais TE, Vogel JH, Chase TR. Multiaxial cycle counting for critical plane methods. *Int J Fatigue* 2003;25:641–7.
- [16] Dang Van K, Papadopoulos I V. High-cycle metal fatigue. Springer; 1999.
- [17] Freitas M, Li B, Santos JLT. Multiaxial fatigue and deformation: testing and prediction. ASTM STP 1387; 2000.
- [18] Gonçalves CA, Araújo JA, Mamiya EN. Multiaxial fatigue: a stress based criterion for hard metals. *Int J Fatigue* 2005;27:177–87.
- [19] Zouain N, Mamiya EN, Comes F. Using enclosing ellipsoids in multiaxial fatigue strength criteria. *Eur J Mech – A, Solids* 2006;25:51–71.
- [20] Mamiya EN, Araújo JA, Castro FC. Prismatic hull: a new measure of shear stress amplitude in multiaxial high cycle fatigue. *Int J Fatigue* 2009;31:1144–53.
- [21] Matsuishi M, Endo T. Fatigue of metals subjected to varying stresses. *Jpn Soc Mech Eng* 1968.
- [22] ASTM E 1049. Practices for cycle counting in fatigue analysis. ASTM Standards v.03.02.
- [23] Meggiolaro MA, Castro JTP, ViDa – Programa para Previsão de Vida à Fadiga sob Carregamentos Complexos, III Simpósio de Análise Experimental de Tensões. PUC-Rio, Brazilian Society of Mechanical Sciences and Engineering; 1995. p. 7–10 (in Portuguese).
- [24] Miranda ACO, Meggiolaro MA, Castro JTP, Martha LF, Bittencourt TN. Fatigue crack propagation under complex loading in arbitrary 2D geometries. In: Applications of automation technology in fatigue and fracture testing and analysis, 4th vol. ASTM STP 1411, West Conshohocken (PA, USA), American Society for Testing and Materials; 2002. p. 120–45.
- [25] Miner MA. Cumulative damage in fatigue. *J Appl Mech* 1945;12:A159–64.
- [26] Bannantine JA, Socie DF. A variable amplitude multiaxial fatigue life prediction method, fatigue under biaxial and multiaxial loading. London: ESIS Publication 10, Mechanical Engineering Publications; 1991. pp. 35–51.
- [27] Coxeter HSM, Greitzer SL. Geometry revisited. Washington (DC): Math. Assoc. Amer; 1967.